VNU Journal of Science: Mathematics - Physics

Journal homepage: https://js.vnu.edu.vn/MaP

Original Article

DFT based Investigation of Structural, Thermodynamic, Mechanical and Electronic Properties of RuVZ (Z: As, Bi, Sb) Half-Heusler Semiconductors

Nenuwe*, Oyindenyifa Nelson and Omagbemı, Oghogho

Department of Physics, Federal University of Petroleum Resources, P. M. B. 1221, Effurun, Delta State, Nigeria

Received 28 February 2022
Revised 7 March 2022; Accepted 7 March 2022

Abstract: Half-Heusler (hH) alloys are an intriguing class of materials with significant potential for applications in spintronics, thermoelectrics, optoelectronics, and magnetoelectronics due to their unique adjustable properties. In this work, we have investigated the structural, thermodynamic, mechanical, and electronic properties of RuVZ (Z: As, Bi, Sb) half-Heusler materials using the density functional theory (DFT) as implemented in the quantum espresso computational suite. The structural, thermodynamic, and mechanical properties were also predicted using the linear response density functional perturbation theory. We observed that the hH alloys are non-magnetic semiconductors and have an indirect narrow band gap. The band gap values and lattice constants for RuVSb and RuVAs cubic crystals are consistent with published reports. RuVBi has a lattice constant of 6.18 Å and a band gap of 0.16 eV. The elastic parameter results obtained satisfy Born's stability requirements, suggesting mechanical stability of the hH materials. All three alloys are found to be ductile. The RuVZ alloys obey the Dulong-Petit law at heat capacity of 74.7, 74.5, and 74.3 J $mol^{-1}K^{-1}$ and temperatures of 556, 754, and 775 K, respectively. The Debye temperature of 353.75K suggests that the RuVAs alloy is the hardest, with a significant Debye sound velocity (2997.12 m/s) and will have high thermal conductivity.

Keywords: Electronic, thermodynamic, mechanical, half-Heusler alloys, RuVBi.

* Corresponding author.
E-mail address: nenuwe.nelson@fupre.edu.ng

https//doi.org/10.25073/2588-1124/vnumap.4705

1. Introduction

Heusler and half-Heusler compounds are a very important class of materials because of their promising potential for applications in spintronics and magnetoelectronics [1, 2]. The full-Heusler (fH) compound with structure X_2YZ was first discovered in 1903 by Heusler Friedrich [3, 4]. The fH alloys crystallize in the $L2_1$ structure and $Fm\bar{3}m$ symmetry group. It has four interpenetrating FCC lattices [5, 6]. Due to their remarkable properties like high curie temperature, strong ferromagnetism even with the absence of elements with magnetic behavior, a lot of attention have been drawn towards finding new materials with tunable multifunctional properties. This search led to the discovery of several variants such as half-Heusler, inverse Heusler and quaternary Heusler [7-10]. The half-Heusler alloys exhibit a chemical formula XYZ with $C1_b$ structure and $F4\bar{3}m$ symmetry group. Particularly, this variant of the Heusler alloys have been found to be useful in thermoelectric and spintronics applications [11-16].

There are several experimental and computational studies reported in publications on half-Heusler alloys [17-35]. Nevertheless, the search for viable half-Heusler semiconductors with suitable properties for specific applications is still needed because some of the already discovered materials have limitations that hinder their suitability for certain applications. In this work, we carefully carry out a density functional theory investigation of structural, thermodynamic, mechanical, and electronic properties of a new class of very promising half-Heusler RuVZ (Z: As, Bi, Sb) materials using the quantum espresso computational suite.

2. Material and Methods

Density functional theory calculations were carried out to study the thermodynamic, structural, mechanical, and electronic properties of RuVZ (Z: As, Bi, Sb) half-Heusler alloys using the quantum espresso (QE) computational code [36, 37]. We used the projector augmented wave (PAW) potentials and generalized gradient approximation (GGA) to treat the Perdew-Burke-Erzherhof (PBE) exchange and correlation between electrons [38-41]. The self-consistent functional (scf) calculations are performed using the Monkhorst-Pack scheme [42] with $8 \times 8 \times 8$ k-points and a converged value of 100 Ry kinetic energy cut-off of the plane wave basis set. We used 10^{-8} Ry as a threshold for convergence of results for the total energy, and Murzari-Vanderbilt smearing width [43] of 0.02 Ry. Atoms in the alloy unit cell were completely relaxed to obtain the equilibrium atomic positions. We used a tetrahedra occupation with a denser k-point mesh of $(25 \times 25 \times 25)$ grid in calculating the electronic density of states. We analysed the alloy properties by fitting the dada set generated from the total energy calculation to the Birch-Murnaghan equation of state [44-46]. We used the XCrysDen software [47] to carefully select a dense high symmetry k-points for the band structure computations. Investigations of the thermodynamic behaviour, mechanical and elastic properties were done by using the Thermo_pw code as a post-proc in QE suite which employs the linear response density functional perturbation theory (DFPT) [48].

3. Results and Discussion

3.1. Structural and Electronic Properties

We investigated RuVZ (Z: As, Bi, Sb) half-Heusler alloys in cubic crystal structure $C1_b$, belonging to space group 216: F-43m. The electronic configuration of the valence shell of these alloys are $6s^2\ 5p^3$, $5s^2\ 5p^3$ and $4s^2\ 4p^3$ for Bi, Sb and As, respectively. While Ru and V are $5s^1\ 4d^7$ and $4s^2\ 3d^3$ respectively.

We studied the α-phase of the structure with X, Y, Z occupying the positions (0.25, 0.25, 0.25), (0.5, 0.5, 0.5) and (0.00, 0.00, 0.00) respectively. The RuVZ alloys crystallize as non-ferromagnetic semiconductor. We confirmed this by applying the well-known Slater-Pauling relation ($M_t = Z_t$ - 18) for half-Heusler alloys. For the alloys we studied, Z_t is 18, making M_t = 0. We computed the structural parameters of RuVZ alloy by carefully optimizing the total energy with respect to the lattice constant and fitted to the third Murnaghan equation of state represented by Eq. (1) [49].

$$E - E_0 = \left[\frac{V_n}{B'} + \frac{V_n}{B'(B'-1)} + \frac{1}{(1-B')}\right] BV_0 \quad (1)$$

B and B' represents the bulk modulus and its derivative. E_0 and V_0 denotes the equilibrium values of energy and volume, respectively. Figure 1 shows the convergence of the lattice constant for RuVBi, RuVSb and RuVAs half-Heuslers. Our calculated values for lattice constants, bulk modulus and the pressure derivative of B are represented in Table 1 alongside with results obtained from both theoretical computations [50, 51] and experiment [52]. For the first time, we have obtained results for the lattice constant, bulk modulus, and its derivative as 6.18 Å, 143.35 GPa and 5.14 respectively, for RuVBi half-Heusler. Also, our calculated values of lattice constants for RuVSb and RuVAs agree with both experiment and other theoretical results. When compared with Chibani *et al*., our results for B and B' are lower for RuVSb and RuVAs. This variation might be as a result of different computational methods employed.

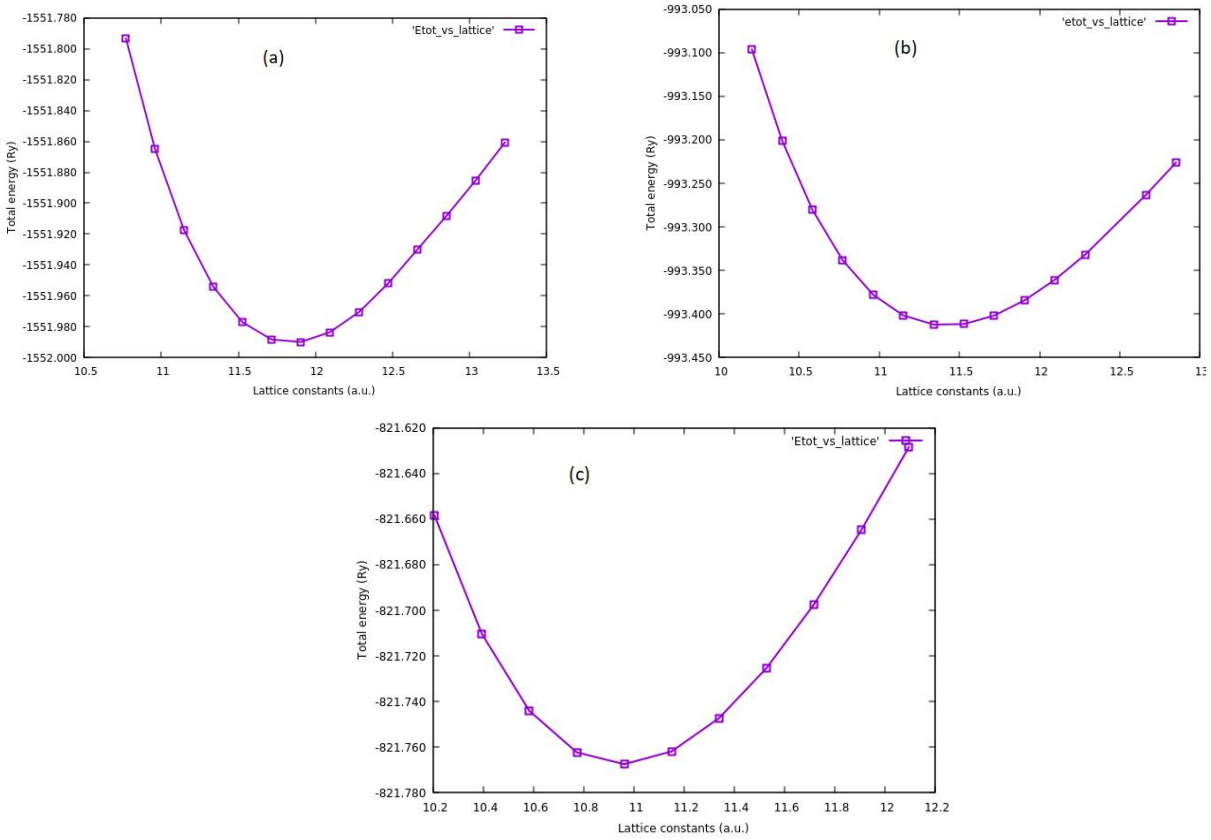

Figure 1. Total energy versus Lattice constant for (a) RuVBi (b) RuVSb (c) RuVAs half-Heusler alloys.

Table 1. Calculated equilibrium lattice constants a_0 (Å), bulk modulus B_0 (GPa) and their pressure derivative and band gap E_g of RuVBi, RuVSb and RuVAs half-heusler alloys compared with previous results.

Alloy	a_0	B_0	B_0'	E_g
RuVBi	6.18*	143.35*	5.14*	0.16*
RuVSb	6.04*, 6.06[a], 5.98[b], 6.02[c], 6.05[d]	163.04* 181.10[b]	4.61* 5.11[b]	0.20*, 0.20[d], 0.19[c] 0.22[d]
RuVAs	5.79*, 5.73[b], 5.76[c], 5.80[d]	183.80* 201.71[b]	4.33* 4.7[b]	0.14*, 0.19[a], 0.24[d], 0.09[b], 0.59[b]

* This work, [a] Ref. [50], [b] Ref. [51], [c] Ref. [53], [d] Ref. [54].

Band structures and density of states provide enough information on electronic properties of solids. In this work, electronic band structure of the investigated half Heusler alloys is determined self-consistently by using their equilibrium lattice parameters along the high symmetry directions in the Brillouin Zone. Figure 2 shows the electronic band structure for RuVBi, RuVSb and RuVAs alloys. The alloys exhibit indirect band gaps between X and L with the conduction band minimum at X and valence band maximum at L. The calculated band gap for these alloys is approximately 0.16, 0.20 and 0.14 for RuVBi, RuVSb and RuVAs, respectively. The band gap value reported in this work for RuVSb alloy agrees with previous results reported in literature. [50, 51, 53, 54]. The band gap obtained for RuVAs agrees with Ref. [50], but slightly different from the values reported in Ref. [53, 54]. The authors in Ref. [50] investigated RuVAs using DFT (with GGA-PBEsol approximation) as implemented in Wien2k code. While the authors in Ref. [53] used an estimated plane wave cut-off energy of 520 eV (38.2 Ry) and convergence threshold of 10^{-5} eV in their DFT calculations as implemented in the VASP code. Authors in Ref. [53] investigated 27 half-Heusler semiconductors using the Heyd-Scuseria-Ernzerhof hybrid functional with the VASP code. Also, they used 520 eV as the cut-off energy for their calculation. In this work, we used 10^{-8} Ry as the convergence threshold and achieved convergence for the plane wave energy cut-off at 100 Ry. The value of the cut-off energy used by the authors in Ref. [53, 54], and the Wien2k code they employed might be responsible for the slight difference in band gaps obtained. For the first time in literature, we have obtained a lattice constant and band gap value of 6.18 Å and 0.16 eV for RuVBi half-Heusler. Figures 3(a – c) show the partial density of states for the studied alloys. The plots clearly indicate that the d-orbitals, doubly degenerate d-e_g, and triply degenerate d-t_{2g} states of the two transition-metal (ruthenium and vanadium atoms) are active around the Fermi level. The maximum contribution to the band gap comes from Ru in the valence band. While, in the conduction band, V (d), d-e_g, d-t_{2g} states are the majority electron contributors to the band gap for all three materials studied.

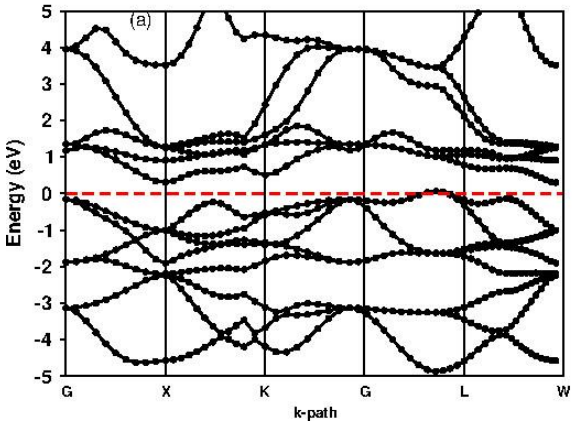

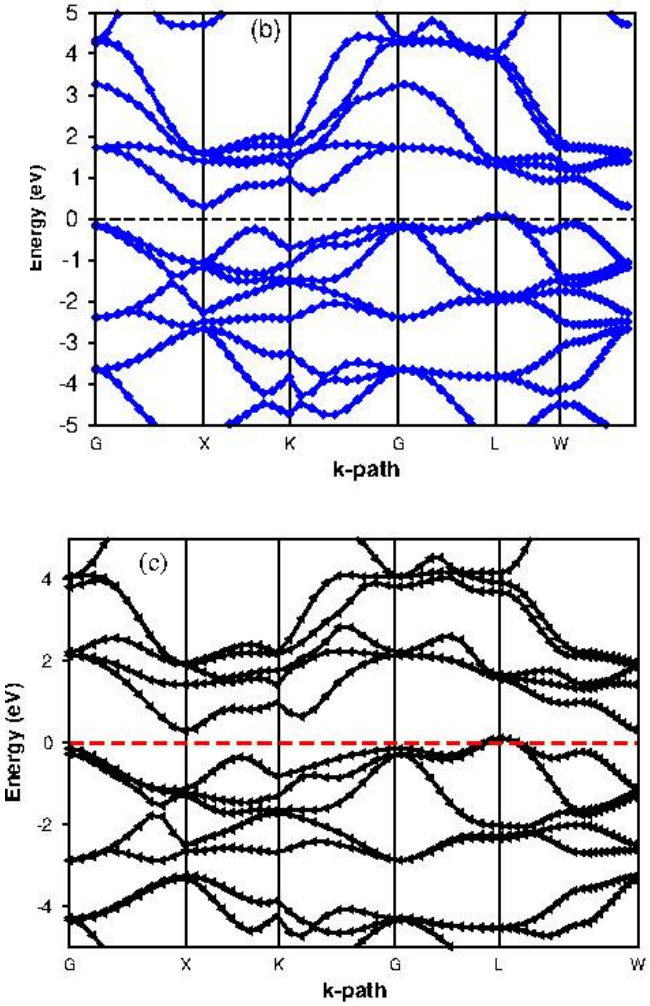

Figure 2. Band structure for (a) RuVBi (b) RuVSb (c) RuVAs half-Heusler alloys using the DFT-GGA approximation.

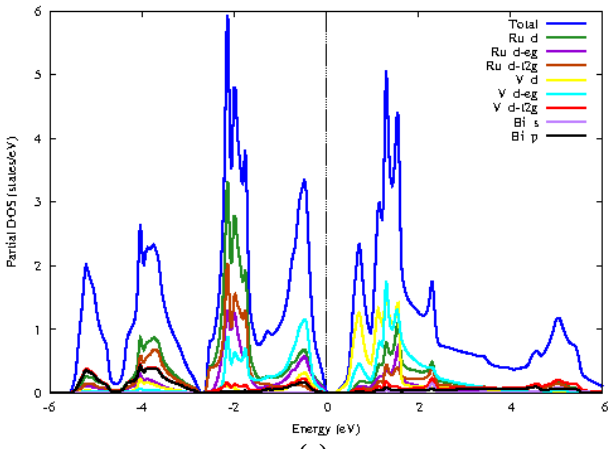

(a)

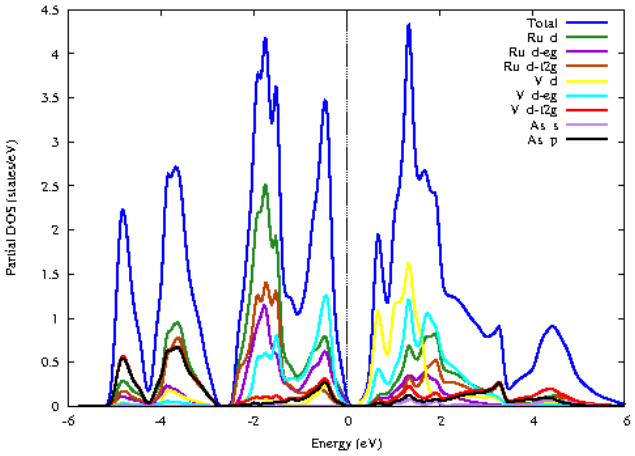

(b)

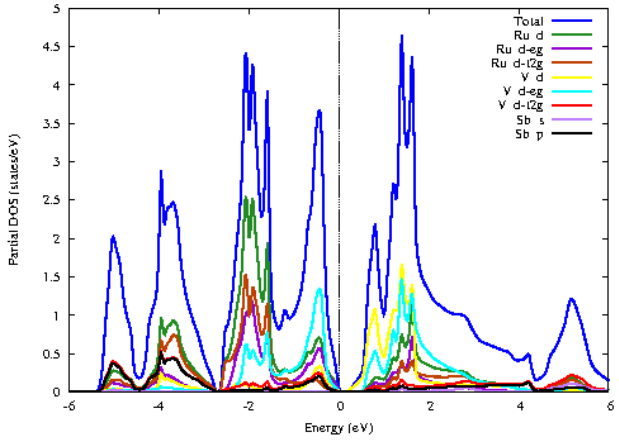

(c)

Figure 3. Partial density of states for (a) RuVBi (b) RuVSb (c) RuVAs half-Heusler alloys.

3.2. Elastic and Mechanical Properties

Studies have demonstrated that understanding the elastic and mechanical properties of materials is crucial in predicting the structural stability for applications. As a result, without initially testing alloys for elastic and mechanical stability, it is impossible to precisely predict their potential applications. In this work, elastic parameters are calculated by the DFPT [48] to examine the elastic and mechanical behaviour of RuVZ alloys. For cubic crystal structures, three independent elastic parameters (C_{11}, C_{12}, and C_{44}) are required to predict elastic stability. The stability conditions are presented as [55]:

$$C_{44} > 0\,;\;\; C_{11} > C_{12}\,;\;\; C_{11} + 2C_{12} > 0 \tag{2}$$

$$C_{12} < B < C_{11} \tag{3}$$

Equations (2) and (3) are known as the Born stability criteria. C_{11} represents a materials' longitudinal stiffness behaviour, C_{12} represents the off-diagonal stiffness characteristics, shear stiffness behaviour is described by C_{44}, and material resistance to external deformation is represented by B. The RuVAs alloy was observed to have the largest value of bulk modulus, followed by RuVSb and RuVBi, as presented

in Table 1. This means that RuVAs is the stiffest of the three alloys and has the highest resistance to external deformation.

We employed the following relations to calculate various elastic parameters such as young modulus (E), bulk modulus (B), and shear modulus (G), Pugh ratio (p), anisotropy factor (A), and Poisson ratio (v) [57].

$$B = \frac{1}{3}(C_{11} + 2C_{12}) \tag{4}$$

$$G = \frac{1}{2}(G_v + G_R) \tag{5}$$

$$E = \frac{9BG}{3B+G} \tag{6}$$

$$G_R = \frac{5(C_{11}-C_{12})C_{44}}{3(C_{11}-C_{12})+4C_{44}} \tag{7}$$

$$G_v = \frac{1}{5}(C_{11} - C_{12} + 3C_{44}) \tag{8}$$

$$A = \frac{2C_{44}}{C_{11}-C_{12}} \tag{9}$$

$$v = \frac{3B-2G}{2(3B+G)} \tag{10}$$

$$p = \frac{B}{G} \tag{11}$$

The Reuss and Voigt approximations of G are G_R and G_v, respectively. The calculated elastic parameters are presented in Table 2. According to these findings, C_{11}, C_{12} and C_{44} for the half-Heusler alloys investigated are positive and meet the elastic stability criteria stated in Eq. (2). In addition, B satisfies the inequality Eq. (3). We observed that RuVAs half-Heusler semiconductor has the highest C_{11}, and therefore, the alloy will be more resistant to unidirectional compression. The Young modulus of a material is the ratio of tensile stress to tensile strain. It is used to figure out how rigid a solid may be. As a result, larger E values indicate stiffer materials. RuVAs is the hardest of the three materials investigated in this work. Shear modulus (G) also describes a material's resistance to plastic deformation. RuVBi, RuVSb, and RuVAs have G values of 17.02, 38.7, and 55.2 GB, respectively. This indicates that RuVBi exhibit the least resistance to plastic deformation, whereas RuVAs has a higher resistance.

Table 2. Calculated elastic parameters (in GPa) at equilibrium volume for cubic RuVBi, RuVSb and RuVAs half-heusler alloys using DFPT.

Alloy	C_{11}	C_{12}	C_{44}	Young modulus (E)	Bulk modulus (B)	Shear modulus (G)	Poisson ratio (v)	B/G	A
RuVBi	202.60	111.90	7.58	48.90	142.15	17.02	0.4406	8.35	0.167
RuVSb	233.30 263.55[b]	128.50 135.41[b]	31.50 53.12[b]	107.50 155.16	163.40	38.70 57.26[b] 50[d]	0.3904	4.22 3.11[b]	0.6011 0.82[b]
RuVAs	241.99 256.27[a] 242.55[d]	153 175.82[a] 164.75[d]	63.70 69.88[a] 123.12[d]	150.30 153.81[a]	182.7 202.64[a]	55.20 55.99[a]	0.3628 0.373[a]	3.31 3.61[a]	1.43 1.73[a]

[a] Ref. [50], [b] Ref. [51], [d] Ref. [54].

Mechanical behaviour of materials such as brittleness and ductility are extremely important during manufacture. As a result, knowing these properties for each material is essential for determining its suitability for various applications. For these two extreme behaviours, a threshold value of 1.75 defined by Pugh in 1954 is utilized as an indicator. If a material's bulk to shear modulus (*B/G*) ratio is more than 1.75, it is considered ductile, while values less than this suggests brittle behaviour. The results reported in Table 2 indicate that all three materials are ductile in nature. Out of the three compounds investigated, RuVBi is the most ductile material. The transverse strain to longitudinal strain ratio is known as the Poisson ratio. It provides data on material stability as well as the types of bonding forces [59]. A higher Poisson ratio indicates that the material is more plastic. Ionic bonded materials have a Poisson ratio of 0.25, covalent bonded materials have a Poisson ratio of 0.1, and materials with a Poisson ratio of 0.25 – 0.5 indicate the presence of a central force in the solid material. Results obtained for RuVBi, RuVSb, and RuVAs are 0.4406, 0.3904, and 0.3628, respectively. This shows that in all three alloys investigated, central forces are dominating. This result agrees with RuVSb and RuVAs values obtained by Chibani et al. [50]. The anisotropy factor (*A*) is another elastic parameter that is relevant in technical applications. It has the potential to alter material microcracks. *A* = 1 indicates that the material is elastically isotropic, while a value of less (or greater) than 1 indicates that the degree of elasticity is anisotropic. The computed *A* for RuVBi and RuVSb in this work is less than 1, but RuVAs is more than 1. As a result, these three alloys are classified as anisotropy materials.

3.3. Thermodynamic Properties

To investigate the thermodynamic properties of RuVZ (Z: As, Bi, Sb), the Quasi-Harmonic Approximation (QHA) was applied against the Harmonic Approximation (HA). The HA lacks the ability to account for phonon-phonon interaction and thermal transport with increase in temperature as such interprets the phonon lifetime as infinite. The QHA addresses these limitations by inserting the x-parameter into the HA of the vibrational Helmholtz energy. Hence, we obtain the QHA expression as:

$$F^{vib}(X,T) = \frac{1}{2}\sum_{qv}\hbar\omega(q,v,X) + K_B T \sum_{qv}\left[1 - exp\left(\frac{-\hbar\omega(q,v,X)}{K_B T}\right)\right] \quad (12)$$

Where *X* represents the volume or lattice parameter, ω represents vibrational frequency, *q* is the wave vector, *T* is the absolute temperature, K_B represents the Boltzmann constant, *v* is the frequency and $\hbar$ is the Planck's constant. One must also note that the QHA do not account for anharmonicity at extremely high temperature above 1000 K. However, between 0 – 800 K investigated in this work, there is enough information to analyze thermodynamic properties and make concrete predictions about these alloys. All computations were carried out under zero pressure and temperatures ranging from 0 to 800 K. The Debye temperature Θ_D, Debye sound velocity V_m, and specific heat capacity with constant volume C_v are the thermodynamic parameters investigated. The Debye temperature is a key fundamental physical variable that is linked to a variety of solid-state properties such as free energy, specific heat, entropy, and melting temperature. The calculated Debye temperature, compressional velocity, shear velocity, bulk velocity, and average sound velocity are all reported in Table 3. We computed the Debye temperature using the relation.

$$\Theta_D = \frac{h}{2\pi K_B}\left(\frac{3n}{4\pi}\frac{N_A\rho}{M}\right) \quad (13)$$

N_A represents Avogadro's number, ρ is density and M represents molecular weight. The average sound velocity is calculated using,

$$V_m = \sqrt[3]{3}\left(\frac{2}{V_G^3}\frac{1}{V_P^3}\right)^{-\frac{1}{3}} \quad (14)$$

We computed the sound velocities using the Navier's equation [60, 61].

$$V_p = \sqrt{\frac{3B+4G}{3\rho}} \tag{15}$$

$$V_G = \sqrt{\frac{G}{\rho}} \tag{16}$$

The molecular weight of RuVBi, RuVSb and RuVAs are 360.99, 273.77 and 226.93, respectively. We observed that the RuVAs material has the fastest sound velocity, while RuVBi has the slowest sound velocity out of the three alloys investigated, as reported in Table 3. This is in accordance with the expectation that lighter material with lighter weight will have a faster sound velocity.

Table 3. Results obtained for the average Debye sound velocity (Vm), Voigt-Reuss-Hill average shear sound velocity (VG), compressional sound velocity (VP) and bulk sound velocity (VB), and the Debye temperature for RuVZ (Z: Bi, Sb, As) alloys using DFPT.

Alloy	m/s				Θ_D (K)	Mass of unit cell (a.m.u.)	Density (kgm^{-3})
	V_G	V_P	V_B	V_m			
RuVBi	1295.53	4031.69	3743.88	1363.08	150.26	360.99	9589.19
RuVSb	2165.64	5107.33	4453.26	2437.37	274.94	273.77	8418.57
RuVAs	2666	5746.05	4851.70	2997.12	353.75	226.93	8139.38

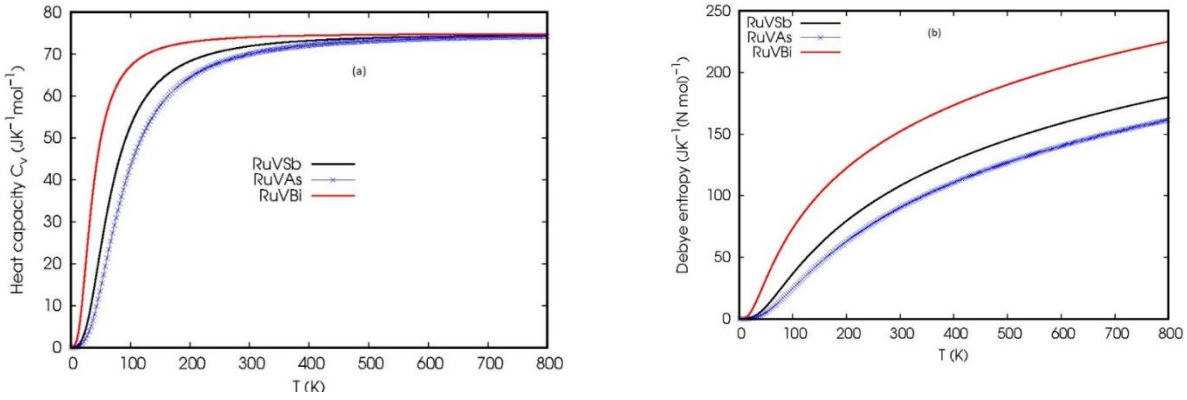

Figure 4. (a) Specific heat capacity C_v and (b) Entropy of RuVBi, RuVSb and RuVAs alloys.

The calculated results for Θ_D are 150.26, 274.94 and 353.75 K for RuVBi, RuVSb and RuVAs, respectively. This is in line with the fact that solid-state molecular weight is inversely proportional to Debye temperature. It is important to note that quantum mechanical effects are negligible above the Debye temperature, whereas quantum mechanical effects play a critical role in understanding the thermodynamic behaviour of materials below the Debye temperature [62]. We predict that RuVAs will be a superior conductor based on the Debye temperature results. As shown in Figure 4(a), the predicted heat capacity C_v values for these three materials increase very fast at low temperatures, then slowly increase at high temperatures, approaching the Petit-Dulong limit [63]. C_v is proportional to T^3 at low temperatures. For RuVBi, RuVSb, and RuVAs, the Dulong-Petit limit is reached at temperatures of around 556, 754, and 775K, with heat capacities of 74.7, 74.5, and 74.3 Jmol^{-1}K^{-1}, respectively. In

addition, when the temperature is increased, we found a rapid and constant increase in entropy of the three compounds as shown in Figure 4(b). The heat capacity with the Dulong-Petit behavior, entropy, and Debye temperature obtained in this work are consistent with other half-Heusler compounds with similar atomic mass. Also, the thermodynamic stability of RuVBi, RuVSb and RuVAs is investigated, and the phonon dispersions are shown in Figures 5 (a– c), respectively. We observed the absence of negative frequencies. This indicates that the alloys investigated are thermodynamically stable.

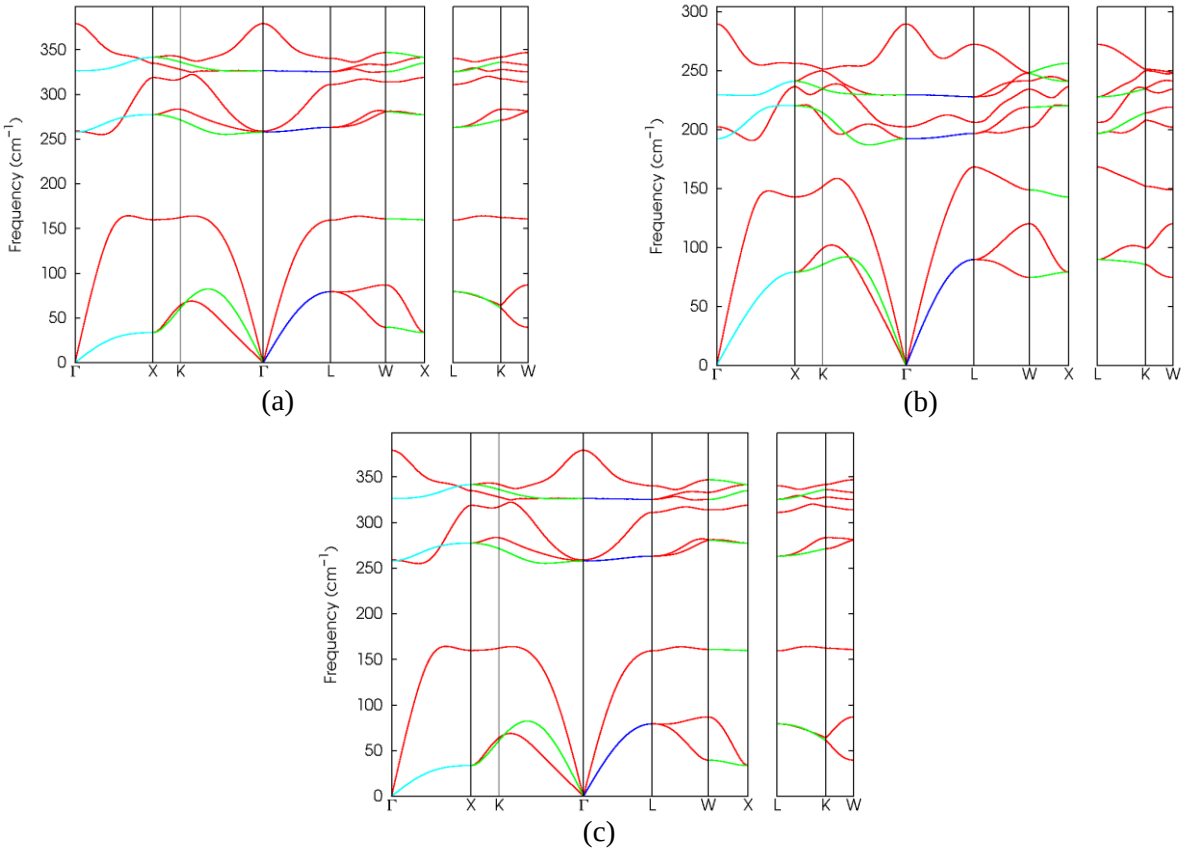

Figure 5. Phonon dispersion of (a) RuVBi (b) RuVSb (c) RuVAs half-Heusler alloys.

4. Conclusions

We investigated the structural, thermodynamic, mechanical, and electronic properties of RuVBi, RuVSb, and RuVAs half-Heusler alloys using density functional theory. All the alloys have zero total magnetic moment and follow the Slater-Pauling rule. The non-magnetic semiconductors RuVBi, RuVSb, and RuVAs were found to have an indirect narrow band gap. The calculated lattice constants and band gaps for RuVSb and RuVAs correspond with previous results in literature. The lattice constant and band gap values calculated for RuVBi alloy are of 6.18 Å and 0.16 eV, respectively. However, no data for RuVBi have been published in the literature. As a result, these findings can be used as a starting point for further research. We employed the QHA and linear response density functional perturbation theory to investigate the thermodynamic, mechanical, and elastic properties of the compounds. Our findings show that all three alloys are ductile, with RuVBi being the most ductile of the three. The

compounds were also found to be thermodynamically stable. The Dulong-Petit limit is achieved at temperatures of roughly 556, 754, and 775 K, with heat capacity of 74.7, 74.5, and 74.3 J mol-1K-1, respectively, while the Debye temperatures for RuVBi, RuVSb, and RuVAs are 150.26, 274.94, and 353.75 K, respectively. These data show that RuVAs will be the best thermal conductor among the three alloys studied, while RuVBi with the lowest thermal conductivity is a better thermoelectric material. We hope that this research will stimulate the interest of experimentalists interesting in fabricating these alloys for further applications in spintronics or magnetoelectronics.

References

[1] I. Zutic, J. Fabian, S.D. Sarma, Spintronics: Fundamentals and Applications, Revs. modern, Phys. Vol. 76, No. 2, 2004, pp. 323, https://doi.org/10.1103/RevModPhys.76.323.

[2] A. Hirohata, K. Takanashi, Future Perspectives for Spintronic Devices, J. Phys. D: Appl. Phys, Vol. 47, No. 19, 2014, pp. 193001, https://doi.org/10.1088/0022-3727/47/19/193001.

[3] F. Heusler, Über Magnetische Manganlegierungen, Verhandlungen der Deutschen Physikalischen Gesellschaft, Vol. 5, 1903, pp. 219.

[4] O. Heusler, Crystal Structure and Ferromagnetism of Manganese-Aluminium-Copper Alloys, Annalen der Physik, Vol. 411, No. 2, 1934, pp. 155-201.

[5] H. Kurt, J. M. D. Coey, Magnetic and Electronic Properties of Thin Films of Mn-Ga and Mn-Ge Compounds with Cubic, Tetragonal and Hexagonal Crystal Structures, in Heusler Alloys, Springer Series Material Science, Vol. 222, 2016, pp. 57-191, https://doi.org/10.1007/978-3-319-21449-8_7.

[6] V. Alijani, J. Winterlik, G. H. Fecher, S. S. Naghavi, C. Felser, Quaternary Half-Metallic Heusler Ferromagnets for Spintronics Applications, Phys. Rev. B, Vol. 83, No. 18, 2011, pp. 184428, https://doi.org/10.1103/PhysRevB.83.184428.

[7] R. A. D. Groot, F. M. Mueller, P. G. V. Engen, K. H. J. Buschow, New Class of Materials: Half-Metallic Ferromagnets, Phys. Rev. Lett, Vol. 50, No. 25, 1983, pp. 2024, https://doi.org/10.1103/PhysRevLett.50.2024.

[8] C. B. Park, H. I. Na, S. S. Yoo, K. S. Park, Electromechanical Properties of Amorphous Indium–Gallium–Zinc-Oxide Transistors Structured with An Island Configuration on Plastic, Appl. Phys. Express, Vol. 9, No. 3, 2016, pp. 031101, https://doi.org/10.7567/APEX.9.031101.

[9] J. P. H. V. Cotrina, F. Garcia, E. R. P. Novais, A. P. Guimarães, Interaction between Magnetic Vortex Cores in a Pair of Nonidentical Nanodisks, J. Appl. Phys, Vol. 115, No. 20, 2014, pp. 203902, https://doi.org/10.1063/1.4878875.

[10] H. X. Liu, T. Kawami, K. Moges, T. Uemura, M. Yamamoto, F. Shi, P. M. Voyles, Influence of Film Composition In Quaternary Heusler Alloy Co_2(Mn, Fe)Si Thin Films on Tunnelling Magnetoresistance of Co_2(Mn, Fe) Si/MgO-based Magnetic Tunnel Junctions, J. Phys. D: Appl. Phys, Vol. 48, No. 16, 2015, pp. 164001, https://doi.org/10.1088/0022-3727/48/16/164001.

[11] W. Everhart, J. Newkirk, Mechanical Properties of Heusler Alloys, Heliyon, Vol. 5, No. 5, 2019, pp. e01578, https://doi.org/10.1016/j.heliyon.2019.e01578.

[12] S. Chen, Z. Ren, Recent Progress of Half-Heusler for Moderate Temperature Thermoelectric Applications, Materials Today, Vol. 16, No. 10, 2013, pp. 387-395, https://doi.org/10.1016/j.mattod.2013.09.015.

[13] H. Xie, H. Wang, Y. Pei, C. Fu, X. Liu, G. J. Snyder, T. Zhu, Beneficial Contribution of Alloy Disorder to Electron and Phonon Transport in Half-Heusler Thermoelectric Materials, Advanced Funct. Mats, Vol. 23, No. 41, 2013, pp. 5123-5130, https://doi.org/10.1002/adfm.201300663.

[14] A. Planes, L. Mañosa, M. Acet, Magnetocaloric Effect and its Relation to Shape-Memory Properties in Ferromagnetic Heusler Alloys, J. Phys: Condens. Matter, Vol. 21, No. 23, 2009, pp. 233201, https://doi.org/10.1088/0953-8984/21/23/233201.

[15] S. Singh, T. M. Bhat, D. C. Gupta, Effect of High Pressure and Temperature on Magneto-Electronic, Thermodynamic, and Transport Properties of Antiferromagnetic HoPdX (X= As, Ge) Alloys, J. Superconduct. Nov. Magn, Vol. 32, No. 7, 2019, pp. 2051-2065, https://doi.org/10.1007/s10948-018-4915-1.

[16] R. Dahal, G. C. Kaphle, Structural, Electronic and Magnetic Properties of XYZ Type Half-Heusler Alloys, J. Nepal Phys, Soc, Vol. 5, No. 1, 2019, pp. 97-102, https://doi.org/10.3126/jnphyssoc.v5i1.26938.

[17] H. Xie, H. Wang, C. Fu, Y. Liu, G. J. Snyder, X. Zhao, T. Zhu, The Intrinsic Disorder Related Alloy Scattering in ZrNiSn Half-Heusler Thermoelectric Materials, Scient. Rep, Vol. 4, No. 1, 2014, pp. 1-6, https://doi.org/10.1038/srep06888.

[18] T. Zhu, C. Fu, H. Xie, Y. Liu, X. Zhao, High efficiency half-Heusler Thermoelectric Materials for Energy Harvesting, Adv. Energy Mats, Vol. 5, No. 19, 2015, pp. 1500588, https://doi.org/10.1002/aenm.201500588.

[19] J. Yang, H. Li, T. Wu, W. Zhang, L. Chen, J. Yang, Evaluation of Half-Heusler Compounds as Thermoelectric Materials Based on the Calculated Electrical Transport Properties, Adv. Funct. Mats, Vol. 18, No. 19, 2008, pp. 2880-2888, https://doi.org/10.1002/adfm.200701369.

[20] Y. Liu, C. Fu, K. Xia, J. Yu, X. Zhao, H. Pan, T. Zhu, Lanthanide Contraction as a Design Factor for High-Performance Half-Heusler Thermoelectric Materials, Adv. Mats, Vol. 30, No. 32, 2018, pp. 1800881, https://doi.org/10.1002/adma.201800881..

[21] T. Fang, X. Zhao, T. Zhu, Band Structures and Transport Properties of High-Performance Half-Heusler Thermoelectric Materials by First Principles, Materials, Vol. 11, No. 5, 2018, pp. 847, https://doi.org/10.3390/ma11050847.

[22] M. J. Winiarski, K. Bilińska, High Thermoelectric Power Factors of P-Type Half-Heusler Alloys YNiSb, LuNiSb, YPdSb, and LuPdSb, Intermetallics, Vol. 108, 2019, pp. 55-60, https://doi.org/10.1016/j.intermet.2019.02.009.

[23] M. K. Yadav, B. Sanyal, First Principles Study of Thermoelectric Properties of Li-based Half-Heusler Alloys, J. Alloys Compds, Vol. 622, 2015, pp. 388-393, https://doi.org/10.1016/j.jallcom.2014.10.025.

[24] A. Berche, J.C. Tedenac, P. Jund, Phase Separation in the Half-Heusler Thermoelectric Materials (Hf, Ti, Zr) NiSn, Scripta. Matrialia, Vol. 139, 2017, pp. 122-125, https://doi.org/10.1016/j.scriptamat.2017.06.036.

[25] C. Fu, S. Bai, Y. Liu, Y. Tang, L. Chen, X. Zhao, T. Zhu, Realizing High Figure of Merit in Heavy-Band P-Type Half-Heusler Thermoelectric Materials, Nature Communications, Vol. 6, No. 1, 2015, pp. 1-7, https://doi.org/10.1038/ncomms9144.

[26] L. Hongzhi, Z. Zhiyong, M. Li, X. Shifeng, L. Heyan, Q. Jingping, W. Guangheng, Electronic Structure and Magnetic Properties of Fe_2YSi (Y= Cr, Mn, Fe, Co, Ni) Heusler alloys: A Theoretical And Experimental Study, J. Phys D: Appl. Phys, Vol. 40, No. 22, 2007, pp. 7121, https://doi.org/10.1088/0022-3727/40/22/039.

[27] S. E. Kulkova, S. V. Eremeev, T. Kakeshita, S. S. Kulkov, G. E. Rudenski, The Electronic Structure and Magnetic Properties of Full-And Half-Heusler Alloys, Mats. trans, Vol. 47, No. 3, 2006, pp. 599-606, https://doi.org/10.2320/matertrans.47.599.

[28] Y. Gupta, M. M. Sinha, S. S. Verma, A First Principle Study of Structural, Electronic, and Vibrational Properties of LuPdBi Half-Heusler Alloy, Physica Status Solidi (B), Vol. 256, No. 10, 2019, pp. 1900117, https://doi.org/10.1002/pssb.201900117.

[29] N. Mehmood, R. Ahmad, Structural, Electronic, Magnetic, and Optical Properties of Half-Heusler Alloys Rumnz (Z= P, As): A First-Principle Study, J. Superconduct, Nov. Magn, Ahmad, Vol. 31, No. 1, 2018, pp. 233-239, https://doi.org/10.1007/s10948-017-4196-0.

[30] A. Planes, L. Mañosa, M. Acet, Magnetocaloric Effect and Its Relation to Shape-Memory Properties in Ferromagnetic Heusler Alloys, J. Phys: Condens. Matter, Vol. 21, No. 23, 2009, pp. 233201, https://doi.org/10.1088/0953-8984/21/23/233201.

[31] R. C. Vivas, S. S. Pedro, C. Cruz, J. C. G. Tedesco, A. A. Coelho, A. M. G. Carvalho, M. S. Reis, Experimental Evidence of Enhanced Magnetocaloric Properties at Room Temperature and Half-Metallicity on Fe2MnSi-based Heusler Alloys, Mats. Chem. Phys, Vol. 174, 2016, pp. 23-27, https://doi.org/10.1016/j.matchemphys.2016.02.045.

[32] G. A. Naydenov, P. J. Hasnip, V. K. Lazarov, M. I. J. Probert, Huge Power Factor In P-Type Half-Heusler Alloys NbFeSb and TaFeSb, J. Phys. Mats, Vol. 2, No. 3, 2019, pp. 035002, https://doi.org/10.1088/2515-7639/ab16fb.

[33] M. Gilleben, R. Dronskowski, A Combinatorial Study of Full Heusler Alloys By First-Principles Computational Methods, J. Comp. Chem, Vol. 30, No. 8, 2009, pp. 1290-1299, https://doi.org/10.1002/jcc.21152.

[34] O. E. Osafile, J. O. Umukoro, Quasi-Harmonic Approximation Of Lattice Dynamics And Thermodynamic Properties Of Half Heusler ScXSb (x= Ni, Pd, Pt) from First Principles, J. Phys: Condens. Matter, Vol. 32, No. 47, 2020, pp. 475504, https://orcid.org/0000-0001-5154-7610.

[35] O. E. Osafile, N. O. Nenuwe, Lattice Dynamics and thermodynamic Responses of XNbSn Half-Heusler Semiconductors: A First-Principles Approach, J. Nigerian Soc. Phys, Sc, Vol. 3, 2021, pp. 121-130, https://doi.org/10.46481/jnsps.2021.174.

[36] P. Giannozzi, S. Baroni, N. Bonini, M. Calandra, R. Car, C. Cavazzoni, R. M. Wentzcovitch, Quantum Espresso: A Modular and Open-Source Software Project For Quantum Simulations Of Materials, J. Phys: Condens. matter, Vol. 21, No. 39, 2009, pp. 395502, https://doi.org/10.1088/0953-8984/21/39/395502.

[37] P. Giannozzi, O. Andreussi, T. Brumme, O. Bunau, M. B. Nardelli, M. Calandra, S. Baroni, Advanced Capabilities for Materials Modelling with Quantum Espresso, J. Phys: Condens. Matter, Vol. 29, No. 46, 2017, pp. 465901, https://doi.org/10.1088/1361-648X/aa8f79.

[38] G. Kresse, D. Joubert, from Ultrasoft Pseudopotentials to the Projector Augmented-Wave Method, Phys. Rev. B, Vol. 59, No. 3, 1999, pp. 1758, https://doi.org/10.1103/PhysRevB.59.1758.

[39] P. E. Blöchl, Projector Augmented-Wave Method, Phys. Rev. B, Vol. 50, No. 24, 1994, pp. 17953, https://doi.org/10.1103/PhysRevB.50.17953.

[40] J. P. Perdew, K. Burke, M. Ernzerhof, Generalized Gradient Approximation made Simple, Phys. Rev. Lett, Vol. 77, No. 18, 1996, pp. 3865, https://doi.org/10.1103/PhysRevLett.77.3865.

[41] K. Burke, J. P. Perdew, M. Ernzerhof, Why Semilocal Functionals Work: Accuracy of the On-Top Pair Density and İmportance of System Averaging, J. Chem. Phys, Vol. 109, No. 10, 1998, pp. 3760-3771, https://doi.org/10.1063/1.476976.

[42] H. J. Monkhorst, J. D. Pack, Special Points for Brillouin-Zone İntegration, Phys. Rev. B, Vol. 13, No. 12, 1976, pp. 5188, https://doi.org/10.1103/PhysRevB.13.5188.

[43] P. L. Silvestrelli, N. Marzari, D. Vanderbilt, M. Parrinello, Maximally Localized Wannier Functions for Disordered Systems: Application to Amorphous Silicon, Solid State Communs, Vol. 107, No. 1, 1998, pp. 7-11, https://doi.org/10.1016/S0038-1098(98)00175-6.

[44] F. D. Murnaghan, Finite Deformations of an Elastic Solid, Amer. J. Maths, Vol. 59, No. 2, 1937, pp. 235-260, https://doi.org/10.2307/2371405.

[45] F. D. Murnaghan, The Compressibility of Media under Extreme Pressures, Proc, Nat. Acad. Sci, Vol. 30, No. 9, 1944, pp. 244.

[46] F. Birch, Finite Elastic Strain of Cubic Crystals, Phys. Rev, Vol. 71, No. 11, 1947, pp. 809, https://doi.org/10.1103/PhysRev.71.809.

[47] A. Kokalj, XCrySDen-A New Program for Displaying Crystalline Structures and Electron Densities, J. Mole. Graphics Model, Vol. 17, No. 3-4, 1999, pp. 176-179, https://doi.org/10.1016/S1093-3263(99)00028-5.

[48] S. Baroni, P. Giannozzi, A. Testa, Green's-Function Approach to Linear Response in Solids, Phys. Rev. Lett, Vol. 58, No. 18, 1987, pp. 1861, https://doi.org/10.1103/PhysRevLett.58.1861.

[49] L. Hao, R. Khenata, X. Wang, T. Yang, Ab Initio Study of the Structural, Electronic, Magnetic, Mechanical and Thermodynamic Properties of Full-Heusler Mn2CoGa, J. Elect. Mat, Vol. 48, No. 10, 2019, pp. 6222-6230, https://doi.org/10.1007/s11664-019-07417-x.

[50] S. Chibani, O. Arbouche, M. Zemouli, Y. Benallou, K. Amara, N. Chami, M. El Keurti, First-Principles İnvestigation of Structural, Mechanical, Electronic, and Thermoelectric Properties of Half-Heusler Compounds RuVX (X= As, P, and Sb), Comp. Condens. Matter, Vol. 16, 2018, pp. e00312, https://doi.org/10.1016/j.cocom.2018.e00312.

[51] T. Fang, X. Zhao, T. Zhu, Band Structures and Transport Properties of High-Performance Half-Heusler Thermoelectric Materials by First Principles, Materials, Vol. 11, No. 5, 2018, pp. 847, https://doi.org/10.3390/ma11050847.

[52] T. Fang, S. Zheng, T. Zhou, L. Yan, P. Zhang, Computational Prediction of High Thermoelectric Performance in P-Type Half-Heusler Compounds with Low Band Effective Mass", Phy. Chem, Vol. 19, No. 6, 2017, pp. 4411-4417, https://doi.org/10.1039/C6CP07897D.

[53] F. Shi, M. S. Si, J. Xie, K. Mi, C. Xiao, Q. Luo, Hybrid Density Functional Study of Bandgaps for 27 New Proposed Half-Heusler Semiconductors, J. Appl. Phys, Vol. 122, No. 21, 2017, pp. 215701, https://doi.org/10.1063/1.4998145.

[54] J. Ma, V. I. Hegde, K. Munira, Y. Xie, S. Keshavarz, D. T. Mildebrath, W. H. Butler, Computational İnvestigation of Half-Heusler Compounds for Spintronics Applications, Phys. Rev. B, Vol. 95, No. 2, 2017, pp. 024411, https://doi.org/10.1103/PhysRevB.95.024411.

[55] C. B. Evers, C. G. Richter, K. Hartjes, W. Jeitschko, Ternary Transition Metal Antimonides and Bismuthides with MgAgAs-type and Filled NiAs-type Structure, J. Alloys Compds, Vol. 252, No. (1-2), 1997, pp. 93-97, https://doi.org/10.1016/S0925-8388(96)02616-3.

[56] M. Born, K. Huang, Clarendon press 1954.

[57] S. F. Pugh, XCII Relations between the Elastic Moduli and the Plastic Properties of Polycrystalline Pure Metals, J. Sci. Vol. 45, No. 367, 1954, pp. 823-843, https://doi.org/10.1080/14786440808520496.

[58] F. Cherifi, Z. Mostefa, A. Boukra, Z. F. Meghoufel, M. Bouattou, A. F. Kadi, F. Terki, Phys. Status Solid, B, 2020, pp. 2000271.

[59] M. Born, K. Huang, Dynamical Theory of Crystal Lattices, Clarendon Press, 1954, https://doi.org/10.1107/S0365110X56002370.

[60] N. O. Nenuwe, E. O. Agbalagba, High-pressure Effect of Elastic and Mechanical Properties of Hexagonal Gallium Nitride, VNU J. Sci.: Maths-Phys, Vol. 37, No. 2, 2021, pp. 49-58, https://doi.org/10.25073/2588-1124/vnumap.4555.

[61] G. N. Greaves, A. L. Greer, R. S. Lakes, T. Rouxel, Poisson's Ratio and Modern Materials, Nature Mats, Vol. 10, No. 11, 2011, pp. 823-837, https://doi.org/10.1038/nmat3134.

[62] I. R. Shein, A. L. Ivanovskii, Elastic Properties of Mono-and Polycrystalline Hexagonal AlB2-Like Diborides of S, P and D Metals from First-Principles Calculations, J. Phys: Condens. Matter, Vol. 20, No. 41, 2008, pp. 415218, https://doi.org/10.1088/0953-8984/20/41/415218.

[63] O. L. Anderson, A Simplified Method for Calculating the Debye Temperature from Elastic Constants, J. Phys. Chem. Solids, Vol 24, No. 7, 1963, pp. 909-917, https://doi.org/10.1016/0022-3697(63)90067-2.

[64] B. A. Shafaay, Structural, Electronic, Mechanical and Thermodynamic Properties of CdS Compound, J. Chem. Bio, Phys. Sci, Vol. 4, No. 4, 2014, pp. 3606-3618,

[65] A.T. Petit, P. L. Dulong, Research on Some Important Points of the Theory of Heat, Ann. Chem. Phys, Vol. 10, 1981, pp. 395.